

Journal of Biomedical Optics

SPIEDigitalLibrary.org/jbo

Multimodal optical microscopy in combination with gold nanorods for cancer cell imaging

Cai-jun Cao
De-rong Li
Chao-xiong Chen
Xiao-yun Yang
Juan Hu
Yong Yang
Chun-yang Zhang

Multimodal optical microscopy in combination with gold nanorods for cancer cell imaging

Cai-jun Cao,^{a*} De-rong Li,^{a*} Chao-xiong Chen,^{a*} Xiao-yun Yang,^{b*} Juan Hu,^a Yong Yang,^a and Chun-yang Zhang^a

^aShenzhen Institutes of Advanced Technology, Chinese Academy of Sciences, Single-Molecule Detection and Imaging Laboratory, Guangdong 518055, China

^bAffiliated Hospital of Guangdong Medical College, Department of Physical Therapy, Zhanjiang 524001, China

Abstract. The multimodal optical imaging technique, which utilizes nonlinear and linear optical processes, plays an important role in biological and biomedical research. As second-order nonlinear phenomenon, the two-photon luminescence (TPL) results from the nonlinear excitation of fluorescent molecules, while the second harmonic generation (SHG) depends on the second order nonlinear polarization, orientation, and noncentrosymmetric properties of molecules. In contrast, the linear resonance light scattering (RLS) occurs when the molecules are excited by a light beam with a wavelength close to their absorption bands. Since SHG, TPL, and RLS involve different kinds of optical processes, they might be used in parallel to provide complementary information about the structure and function of cells and tissues. Herein, we develop for the first time a multimodal optical microscopy with the capability of simultaneous SHG, TPL, and RLS imaging. We analyze theoretically and demonstrate experimentally the near-infrared irradiation-induced SHG, TPL, and RLS from the gold nanorods with nanometer spatial resolution. With the gold nanorods as the contrast agents, we further demonstrate the simultaneous SHG, TPL, and RLS imaging of A431 human epithelial skin cancer cells. This multimodal optical microscopy might provide a reliable and complementary approach for biological and biomedical research. © 2012 Society of Photo-Optical Instrumentation Engineers (SPIE). [DOI: 10.1117/1.JBO.17.12.126002]

Keywords: multimodal optical microscopy; two-photon luminescence; second harmonic generation; resonance light scattering; gold nanorods; cancer cells.

Paper 12601 received Sep. 11, 2012; revised manuscript received Nov. 4, 2012; accepted for publication Nov. 8, 2012; published online Dec. 3, 2012.

1 Introduction

Multimodal optical imaging technique based on linear and nonlinear optical processes has wide applications in biological and biomedical research and plays an important role in the study of cells and tissues as well as *in vivo* imaging.¹⁻⁴ To date, great efforts have been put into the development of various multimodal optical techniques,¹⁻⁴ such as the combination of second harmonic generation (SHG) and two-photon luminescence (TPL) for the imaging of cells and extracellular matrix,¹ the combination of optical coherence tomography (OCT) and SHG for the imaging of collagen,² the combination of OCT and TPL for the imaging of cancer cells and adipose tissue,³ and the combination of Plasmon resonance Rayleigh scattering and surface-enhanced Raman scattering for the study of yeast cells.⁴ However, the multimodal optical microscopy with the combination of SHG, TPL, and resonance light scattering (RLS) has never been reported so far.

As a three-dimensional imaging technology based on the nonlinear excitation of fluorophores, TPL is particularly suitable for biomedical research because of its inherent advantages of three-dimensional resolution, less photobleaching, and long depth penetration.⁵⁻⁷ Two-photon excitation arises from the simultaneous absorption of two photons in a single quantized event, and the wavelength of two-photon excitation is about

twice that required for single-photon excitation.^{5,8,9} As a younger sibling of TPL, SHG is a new high-resolution optical imaging tool for the visualization of cells and tissues due to its elimination of out-of-plane photobleaching.¹⁰⁻¹² SHG is a nonlinear optical effect whereby incident light is converted to the light of exactly half the wavelength.¹¹ In addition, SHG strongly depends on the defects and the small deviations from the symmetric shape.^{13,14} Recently, as a linear optical imaging tool, RLS has been employed to image cancer cells and tissues.¹⁵⁻¹⁸ When bio-assemblies and aggregation species are excited by a light beam with a wavelength close to their absorption bands, the enhanced RLS signal is observed.¹⁹⁻²² Since TPL, SHG, and RLS involve different kinds of optical processes, they might be used in parallel to provide complementary information about the structure and the function of cells and tissues.

Herein, we develop a multimodal optical microscopy that combines three kinds of different optical processes for simultaneous SHG, TPL, and RLS imaging with high spatial resolution. The transverse spatial resolution might reach 175, 202, and 292 nm for SHG, TPL, and RLS imaging, respectively. The gold nanoparticles have been reported to possess the second harmonic effect, two-photon excitation, and strong light scattering,²³⁻²⁷ making them excellent contrast reagents for simultaneous SHG, TPL, and RLS imaging. In addition, the gold nanoparticles have significant advantages of excellent biocompatibility, nontoxicity, and good resistance to the photobleaching,²⁸ making them good markers for cancer cell imaging. In this research, simultaneous SHG, TPL, and RLS imaging of A431

*These authors contributed equally to this work.

Address all correspondence to: Chun-yang Zhang, Shenzhen Institutes of Advanced Technology, Chinese Academy of Sciences, Single-Molecule Detection and Imaging Laboratory, Guangdong 518055, China. Tel: +86 755 86392211; Fax: +86 755 86392299; E-mail: zhangcy@siat.ac.cn

human epithelial skin cancer cells are obtained using the gold nanorod-conjugated anti-epidermal growth factor receptor (anti-EGFR) antibodies.

2 Experimental Section

2.1 Setup of Multimodal Optical Microscopy

The experimental setup of multimodal optical microscopy is illustrated in Fig. 1. A tunable mode-locked Ti:sapphire laser (Chameleon ultra II, Coherent, Inc.) was used as the excitation source, and it operated at the wavelength of 808 nm with a pulse duration of 140 fs and a pulse repetition rate of 80 MHz. The incident polarization direction and power were controlled by a half-wave plate and a Glan-Laser polarizer. The sample was placed in the focal plane of the objective using a three-dimensional micro-displacement. The pulse energy of the laser beam was 1.25×10^{-10} J, and the energy density of laser beam was 1 mJ/cm^2 . The laser beam was collimated, reflected by a dichroic mirror (10SWF-750-B, Newport), focused by an oil-immersion $100 \times /1.49$ NA objective lens (Olympus America, Inc., Melville, New York), and scanned the sample with a set of two-dimensional scanning galvanometer (6215H, Cambridge). The emitted lights were collected by three channels of RLS, TPL, and SHG, respectively. In RLS channel, resonance scattering light passed through a long-wave-pass optical filter (10LWF-750-B, Newport), and was detected by a photomultiplier tube (PMT, H10492-011, Hamamatsu). In TPL and SHG channels, the two-photon and second harmonic lights were epi-collected, separated by a dichroic mirror (10Z20ER.1, Newport), passed through two optical filters (10LWF-500-B and 10BPF70-400, Newport), and were detected by two PMTs (H10492-003, Hamamatsu), respectively. The data from three channels were acquired simultaneously, and the images were reconstructed in real time with a Labview data acquisition card (PCI-6132, National Instruments). The spectrometer (MAYA2000-PRO, Ocean Optics) was used to measure the emission spectrum of gold nanorods.

2.2 Characterization of Gold Nanorods

The gold nanorods were obtained from J & K Scientific Ltd. (Beijing, China). The extinction spectrum of gold nanorods was recorded on a PerkinElmer Lambda 25 UV/vis spectrophotometer (PerkinElmer, Inc. Waltham). The size and shape

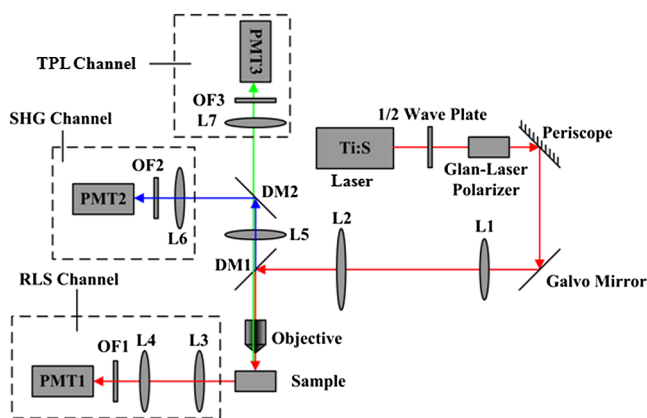


Fig. 1 Schematic illustration of multimodal optical microscopy for simultaneous SHG, TPL, and RLS imaging. L, len; DM, dichroic mirror; OF, optical filter; PMT, photomultiplier tube.

distribution of gold nanorods were determined by the transmission electron microscopy (JEOL Ltd., Tokyo, Japan).

2.3 Preparation of Gold Nanorod-Conjugated Anti-EGFR Antibodies

The gold nanorod-conjugated anti-EGFR antibodies were prepared according to the method described by Huang²⁹ and Wang.³⁰ Briefly, the gold nanorods were centrifuged at 8000 rpm twice to remove the extra free cetyltrimethyl ammonium bromide (CTAB). To reverse the surface charge of gold nanorods,³¹ polystyrene sulfonate (PSS, 10 mg/mL in 1 M NaCl, Sigma) was added to the solution of gold nanorods with a volume ratio of 1 : 10 under vigorous stirring for 3 h. The gold nanorods were further washed twice with water to remove the extra PSS, followed by being resuspended in N-(2-hydroxyethyl) piperazine-N'-2- ethanesulfonic acid (HEPES, 40 mM, pH = 7.4, Sigma). The PSS-capped gold nanorods and the monoclonal anti-EGFR antibodies (Clone 29.1.1, Sigma) were then mixed at a volume ratio of 1 : 1 and allowed to interact in HEPES buffer at room temperature for 45 min. For the control group, the nonspecific antibodies (monoclonal MOPC 21, Sigma) were used in place of the anti-EGFR antibodies. Finally, polyethyleneglycol (PEG, 10 mg/mL in PBS, Sigma) was added to the mixture with a final concentration of 0.2 mg/mL for stability, and the gold nanorod-conjugated antibodies were further centrifuged to remove the free reactants.

2.4 Cell Culture and Incubation of Cancer Cells with Gold Nanorod-Conjugated Antibodies

A431 human epithelial skin cancer cells (cell bank of Chinese Academy of Sciences, Shanghai, China) were cultured in Dulbecco's modification of Eagle's medium (DMEM, Gibco) plus 5% fetal bovine serum (FBS, Gibco) at 37°C in a humidified atmosphere of 5% CO₂. The cells were harvested using trypsin, and resuspended in 1× PBS buffer at a concentration of approximately 1.0×10^6 cells/mL. Then the cells were incubated with either gold nanorod-conjugated anti-EGFR antibodies or gold nanorod-conjugated nonspecific antibodies at a volume ratio of 1 : 1 for 45 min. Followed by being centrifuged at 200 g for 5 min to remove the unbound nanorods, the labeled cells were resuspended in a solution of collagen with a final concentration of approximately 5.0×10^6 cells/mL. At last, the labeled cells were pipetted into a 120- μm spacer (Molecular Probes, Inc., Eugene) and sealed with a glass coverslip for subsequent imaging.

3 Results and Discussions

3.1 Characterization of Gold Nanorods

For simultaneous SHG, TPL, and RLS imaging, a suitable contrast reagent should be carefully selected. Figure 2(a) shows the TEM image of gold nanorods. The gold nanorods had an average length of 40 ± 3 nm and an average width of 10 ± 1 nm. In the near-infrared region, the gold nanorods demonstrated the localized surface plasmon resonances,³² and its longitudinal plasmon resonance was centered at 808 nm [Fig. 2(b)]. In this research, the gold nanorods were employed as the contrast agents for simultaneous SHG, TPL, and RLS imaging of A431 skin cancer cells. First of all, we analyzed theoretically (Fig. 3) and demonstrated experimentally (Fig. 4) that the near-infrared

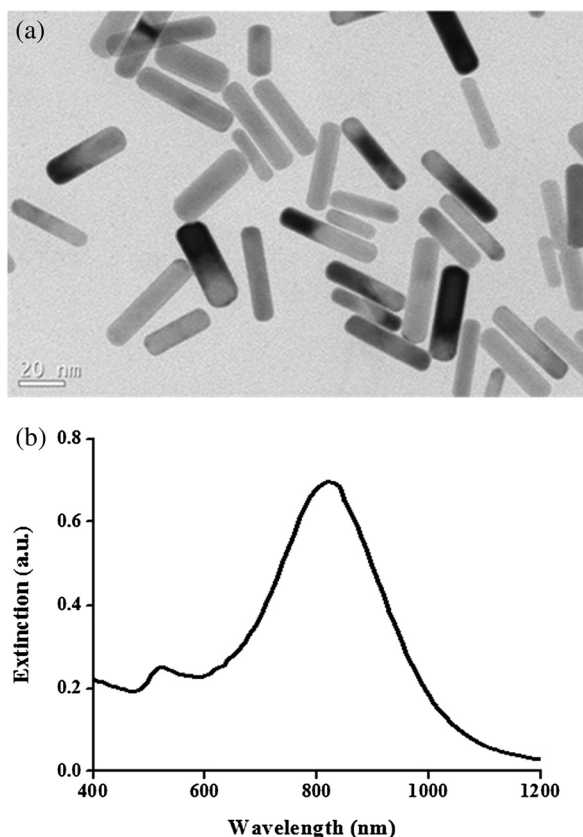


Fig. 2 Characterization of gold nanorods. (a) TEM image of gold nanorods. (b) Absorption spectrum of gold nanorods.

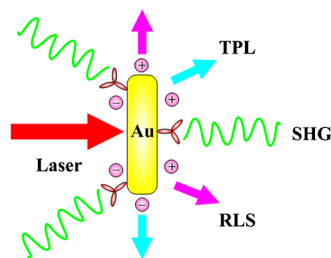


Fig. 3 Illustration of near-infrared irradiation-induced SHG, TPL, and RLS from the gold nanorod.

irradiation might induce SHG, TPL, and RLS from gold nanorods simultaneously.

3.2 Near-Infrared Irradiation-Induced SHG, TPL, and RLS from Gold Nanorods

We first investigated theoretically the factors that influenced the SHG, TPL, and RLS from the gold nanorods (Fig. 3). Near-infrared irradiation induced the excitation of the localized surface plasmon resonances, resulting in RLS. The scattering of light by very small subwavelength-sized particles was well described by Rayleigh theory.^{33,34} For light vertically polarized and perpendicular to the scattering plane, the RLS intensity I_{RLS} is given by the Rayleigh expression:

$$I_{\text{RLS}} \propto \frac{16\pi^2 s^6 n^4 I_{\text{in}}}{r^2 \lambda^4} \left| \frac{m^2 - 1}{m^2 + 2} \right|^2, \quad (1)$$

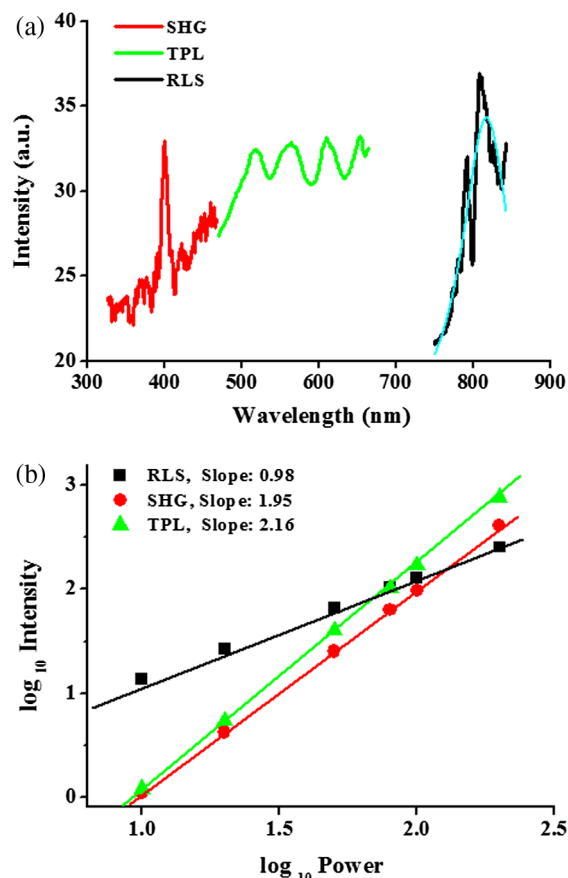


Fig. 4 (a) Emission spectra of SHG (red line), TPL (green line), and RLS (black line) at the excitation wavelengths of 808 nm. Each emission spectrum has been averaged across five measurements acquired at different x-y locations of gold nanorods. (b) Dependence of SHG (red ●), TPL (green ▲) and RLS (black ■) upon the excitation power.

where s is the size of nanorods, n is the refractive index surrounding the nanorods, m is the refractive index of nanorods at the excitation wavelength, r is the distance between the nanorod and the detector, λ is the wavelength of the incident light, and I_{in} is the incident laser intensity. Based on Eq. (1), the RLS intensity I_{RLS} was linearly dependent on the impinging laser intensity, the size, and the aggregation of gold nanorods.²⁷

Together with their linear optical property, the nonlinear optical property of gold nanorods offered great promise for biological applications.^{23,25} Owing to both the localized surface plasmon resonances and the nanomorphology, the gold nanorods might emit SHG.²⁵ The SHG intensity I_{SHG} is proportional to the squared second order nonlinear polarization $\chi^{(2)}$ and the particle dipole $Q^{(2)}(2\omega)$ in the case of metallic nanoparticles,^{14,25}

$$I_{\text{SHG}} \propto [Q^{(2)}(2\omega)]^2 \propto [f(2\omega)]^2 [f(\omega)]^4 I_{\text{in}}^2, \quad (2)$$

where $Q^{(2)}(2\omega)$ is defined as

$$Q^{(2)}(2\omega) \propto f(2\omega) \chi^{(2)} I_{\text{in}}, \quad (3)$$

where $f(\omega)$ is the local field enhancement factor at the fundamental frequency, and $f(2\omega)$ is the local field enhancement factor at the second harmonic frequency. Based on Eq. (2), the second harmonic intensity I_{SHG} strongly depended on the

incident laser intensity I_{in} , and the SHG was resonantly enhanced by the localized surface plasmon resonances in the preferentially excited nanorods.²⁵

The gold nanorods emitted strong photoluminescence under two-photon excitation.³⁵ The two-photon absorption-induced electronic transition from the d -band to the sp -band generated an electron-hole pair, and the subsequent relaxation and recombination of electron-hole pairs led to the TPL emission.³⁶ The efficient TPL resulted from the local field enhancement induced by the surface plasmon.^{23,24} The TPL intensity I_{TPL} is defined as⁹

$$I_{TPL} \propto nPR[f(\omega_L)]^2, \quad (4)$$

where n is the number of adsorbed nanorods, P is the radiative quantum yield of nanorods, and $f(\omega_L)$ is the local field factor of radiation. The excitation rate (R) is given by

$$R = \delta[f(\omega)]^4 I_{in}^2, \quad (5)$$

where δ is the two-photon absorption cross-section of nanorods. Based on Eqs. (4) and (5), the incident laser intensity I_{in} played a dominant role in the TPL efficiency, and the largest enhancement occurred when the incident light coupled with the longitudinal surface plasmon of gold nanorods.

We further demonstrated the near-infrared irradiation-induced SHG, TPL, and RLS from gold nanorods experimentally. Figure 4(a) shows the emission spectra of SHG, TPL, and RLS at the excitation wavelength of 808 nm, respectively. The SHG emission spectrum of gold nanorods was in the range from 330 to 460 nm with a peak of 404 nm [Fig. 4(a)]. This result was in accordance with the theory that the emission wavelength of SHG was exactly one half wavelength of incident light.²⁵ The emission spectrum of TPL was in the range from 470 to 660 nm with two peaks of 517 and 651 nm [Fig. 4(a)], which resulted from the electron-hole radiative recombination near the X and L symmetry.³⁷ The RLS spectrum was measured at different excitation wavelengths and fitted to the Lorentzian calculation. The emission spectrum of RLS was in the range from 750 to 840 nm with a strong peak of 809 nm [Fig. 4(a)], which was very close to the excitation wavelength of 808 nm. This result was in agreement with the previous research that the electrons in the gold oscillated at the same frequency as the incident wave.^{33,34}

Previous research demonstrated that the nonlinear processes were particularly sensitive to the plasmon resonances because of their quadratic dependence on the intensity.^{23,25} To determine the dependence of SHG, TPL, and RLS upon the excitation power, the gold nanorods were sparsely deposited on a glass slide, and a single emission spot of SHG, TPL, and RLS imaging was examined, respectively. Figure 4(b) shows the dependence of SHG, TPL, and RLS upon the excitation power. According to Eqs. (2), (4), and (5), the intensity of both SHG and TPL strongly depended on square of incident field intensity.^{23,25} The quadratic dependence of TPL intensity upon the incident power had an average slope value of 2.16 [Fig. 4(b)], suggesting the two-photon process of TPL.²³ In addition, the nearly quadratic dependence of SHG intensity upon the incident power had an average slope value of 1.95 [Fig. 4(b), indicating a characteristic of second order nonlinear process of SHG.²⁵ According to Eq. (1), the intensity of RLS was linearly dependent on the impinging laser intensity.^{33,34} The linear dependence of RLS intensity upon the incident power had an average slope value

of 0.98 [Fig. 4(b)], further confirming the linear process of RLS.¹⁸

3.3 Spatial Resolution of Multimodal Optical Microscopy

The plasmon resonance of gold nanorods in the near infrared region made them ideal contrast agents for SHG, TPL, and RLS imaging.^{23,25,27} Previous research demonstrated the enhanced spatial resolution for both SHG and TPL imaging because of their nonlinear dependence upon the excitation power,^{38,39} while the resolution of linear scattering was restricted to the diffraction limit.⁴⁰ To determine the spatial resolution of this multimodal optical microscopy experimentally, the gold nanorods were imaged by SHG, TPL, and RLS, respectively. The SHG, TPL, and RLS images of gold nanorods are presented in the left panel of Fig. 5(a)–5(c), respectively. The zoom-in images of a typical nanorod are shown in the right panel of

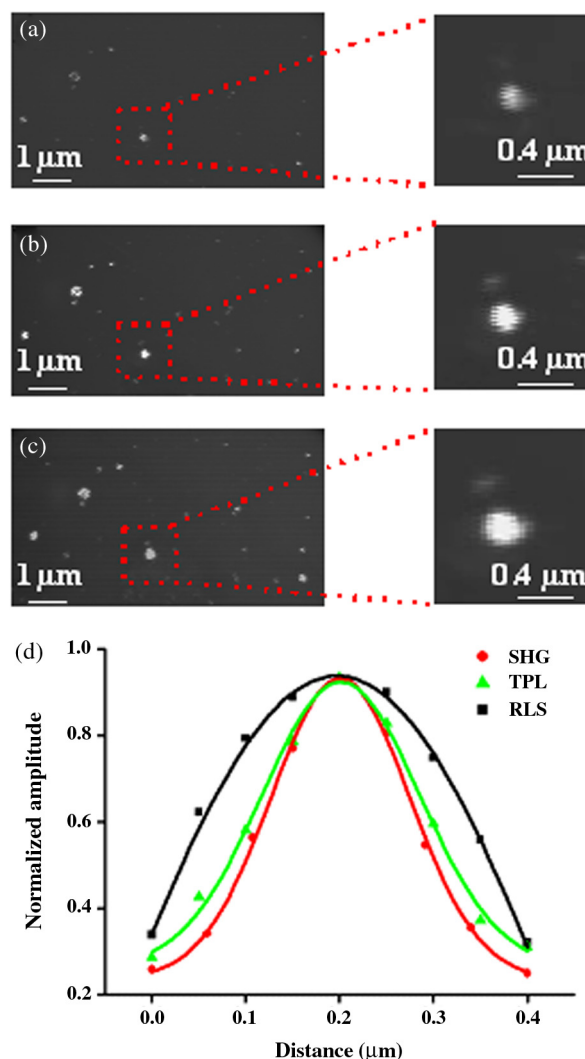


Fig. 5 Transverse spatial resolution of SHG, TPL, and RLS imaging. (a) SHG imaging of gold nanorods. (b) TPL imaging of gold nanorods. (c) RLS imaging of gold nanorods. The zoom-in images of a highlighted single bright spot are shown in the right panel. (d) Gaussian amplitude curve fitting of measured point spread function of SHG (red ●), TPL (green ▲), and RLS (black ■) signals obtained from a typical nanorod, respectively.

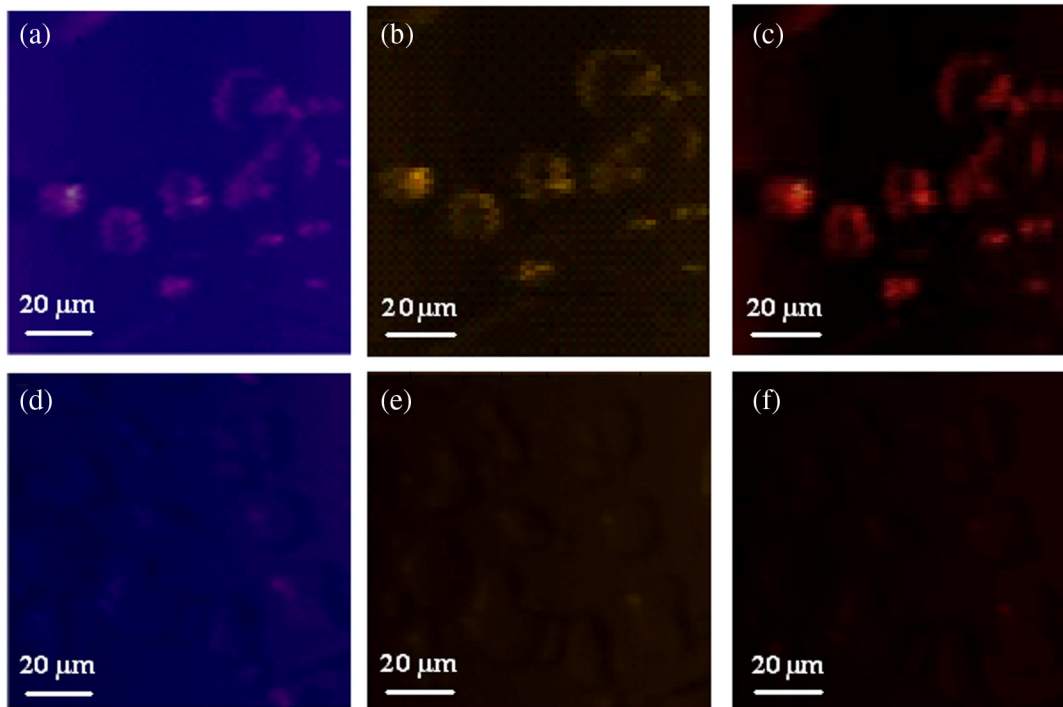


Fig. 6 Simultaneous SHG, TPL, and RLS imaging of A431 human epithelial skin cancer cells. (a–c) SHG image (a), TPL image (b), and RLS image (c) of cancer cells incubated with the gold nanorod-conjugated anti-EGFR antibodies. (d–f) SHG image (d), TPL image (e), and RLS image (f) of cancer cells incubated with the gold nanorod-conjugated nonspecific antibodies. The image size is $100 \times 100 \mu\text{m}$. The scale bar is $20 \mu\text{m}$.

Fig. 5(a)–5(c) as well. The Gaussian amplitude fitting of the measured point spread function of SHG, TPL, and RLS signals is shown in Fig. 5(d). Based on the calculation by the full wave at half maximum (FWHM) of the point spread function,^{41,42} the resolution of nonlinear SHG and TPL imaging was estimated to be 175 and 202 nm, respectively, and the resolution of linear RLS imaging was estimated to be 292 nm (near diffraction limit). In addition, the spatial resolutions were also measured by using a N.A. (1.2) oil objective. The resolutions of SHG, TPL, and RLS were estimated to be 213, 256, and 354 nm, respectively. Notably, the resolutions of SHG, TPL, and RLS were comparable to or even much higher than those reported in the previous researches.^{23,38,43} For example, the resolution of SHG was 200 nm for the imaging of star-shaped golds,³⁸ the resolution of TPL was 300 nm for the imaging of blood vessels,²³ and the Rayleigh scattering displayed submicrometer resolution for the imaging of single-walled carbon nanotubes.⁴³ The high spatial resolution of this multimodal optical microscopy offered great promise for further applications in biological and biomedical research.

3.4 Simultaneous SHG, TPL and RLS Imaging of Cancer Cells

This multimodal optical microscopy was further used for simultaneous SHG, TPL, and RLS imaging of A431 human epithelial skin cancer cells. Figure 6 shows the SHG, TPL, and RLS images of cancer cells incubated with the gold nanorod-conjugated anti-EGFR antibodies and nonspecific antibodies, respectively, at the excitation wavelength of 808 nm. The bright rings were observed in the SHG [Fig. 6(a)], TPL [Fig. 6(b)], and RLS [Fig. 6(c)] imaging, respectively. These bright rings resulted from the aggregates of gold nanorods on the surface of cancer cells due to the specific interaction of EGFR

antibodies with the EGFR receptors on the cell membrane. These results were in agreement with the previous research about a characteristic bright ring in the confocal reflectance imaging of cancer cells using spherical gold nanoparticle-labeled anti-EGFR antibodies.⁴⁴ Under the same laser power, the images of cancer cells in the control group with the treatment of gold nanorod-conjugated nonspecific antibodies are presented in Fig. 6(d)–6(f). There were no characteristic bright rings of EGFR labeling appeared in the SHG, TPL, and RLS images in the control group because the nonspecific antibodies could not bind the EGFR receptors on the cell membranes. The blurred spots in the images of Fig. 6(d)–6(f) might result from the nonspecific attachment of a few gold nanorods to the cell membranes, but they were negligible in comparison with the bright rings in the cancer cells incubated with the gold nanorod-conjugated anti-EGFR antibodies [Fig. 6(a)–6(c)]. The signals of SHG, TPL, and RLS from the cancer cells incubated with the gold nanorods-conjugated anti-EGFR antibodies were so strong that they could be easily observed even using the low excitation power of 10 mW. Importantly, this is the first demonstration of simultaneous SHG, TPL, and RLS imaging of cancer cells. It should be noted that the gold nanorods may not be suitable contrast agents for *in vivo* bioimaging because of the essential opaqueness of tissues and the strong absorbance of hemoglobin in the wavelength range of 330 to 460 nm and 470 to 660 nm. For future practical applications, we might use the quantum dots as the contrast agents for *in vivo* imaging.^{45,46}

4 Conclusions

In summary, we have developed for the first time a multimodal optical microscopy for simultaneous SHG, TPL, and RLS imaging of cancer cells. In this research, we had successfully combined SHG, TPL, and RLS imaging, which involved different

kinds of optical processes, into one unitary system using near-infrared single-wavelength excitation. In addition, we analyzed theoretically and demonstrated experimentally the near-infrared irradiation-induced SHG, TPL, and RLS from the gold nanorods with nanometer spatial resolution. More importantly, we demonstrated the simultaneous SHG, TPL, and RLS imaging of A431 human epithelial skin cancer cells using the gold nanorod-conjugated anti-EGFR antibodies. This multimodal optical microscopy with the capability of simultaneous SHG, TPL, and RLS imaging might provide a reliable and complementary approach for biological and biomedical research.

Acknowledgments

This work was supported by the National Basic Research Program 973 (Grant Nos. 2011CB933600 and 2010CB732600), the National Natural Science Foundation of China (Grant Nos. 21075129 and 11004213), the Award for the Hundred Talent Program of the Chinese Academy of Science, the Guangdong Innovation Research Team Fund for Low-cost Healthcare Technologies, the Natural Science Foundation of Shenzhen City (Grant No. JC201005270327A), and the Fund for Shenzhen Engineering Laboratory of Single-molecule Detection and Instrument Development [Grant No. (2012) 433].

References

1. A. Zoumi et al., "Imaging cells and extracellular matrix in vivo by using second-harmonic generation and two-photon excited fluorescence," *Proc. Nat. Acad. Sci. U. S. A.* **99**(17), 11014–11019 (2002).
2. Y. Jiang et al., "High resolution second-harmonic optical coherence tomography of collagen in rat tail tendon," *Appl. Phys. Lett.* **86**(13), 133901–133903 (2005).
3. J. F. Xi et al., "Integrated multimodal endomicroscopy platform for simultaneous en face optical coherence and two-photon fluorescence imaging," *Opt. Lett.* **37**(3), 362–364 (2012).
4. K. M. Syamala et al., "Inhibition assay of yeast cell walls by plasmon resonance Rayleigh scattering and surface-enhanced Raman scattering imaging," *Langmuir* **28**(24), 8952–8958 (2012).
5. W. Denk et al., "Two-photon laser scanning fluorescence microscopy," *Science* **248**(4951), 73–76 (1990).
6. M. Rubart, "Two-photon microscopy of cell and tissue," *Circ. Res.* **95**(12), 1154–1166 (2004).
7. G. Alexandrakis et al., "Two-photon fluorescence correlation microscopy reveals the two-phase nature of transport in tumors," *Nat. Med.* **10**(2), 203–207 (2004).
8. M. D. Cahalan et al., "Two-photon tissue imaging: seeing the immune system in a fresh light," *Nat. Rev. Immunol.* **2**(11), 872–880 (2002).
9. A. Diaspro et al., "Two-photon fluorescence excitation and related techniques in biological microscopy," *Q. Rev. Biophys.* **38**(2), 97–166 (2005).
10. W. R. Zipfel et al., "Nonlinear magic: multiphoton microscopy in the biosciences," *Nat. Biotechnol.* **21**(11), 1369–1377 (2003).
11. S. Tang et al., "Effect of pulse duration on two-photon excited fluorescence and second harmonic generation in nonlinear optical microscopy," *J. Biomed. Opt.* **11**(2), 020501 (2006).
12. R. Yuste, "Fluorescence microscopy today," *Nat. Med.* **2**(12), 902–904 (2005).
13. P. A. Franken et al., "Generation of optical harmonics," *Phys. Rev. Lett.* **7**(4), 118–119 (1961).
14. P. J. Campagnola et al., "Second-harmonic imaging microscopy for visualizing biomolecular arrays in cells, tissues and organisms," *Nat. Biotechnol.* **21**(11), 1356–1360 (2003).
15. R. Hu et al., "metallic nanostructures as localized plasmon resonance enhanced scattering probes for multiplex dark-field targeted imaging of cancer cells," *J. Phys. Chem. C.* **113**(7), 2676–2684 (2009).
16. K. Aslan et al., "Plasmon light scattering in biology and medicine: new sensing approaches, visions and perspectives," *Curr. Opin. Chem. Biol.* **9**(5), 538–544 (2005).
17. J. Yguerabide et al., "Resonance light scattering particles as ultrasensitive labels for detection of analytes in a wide range of applications," *J. Cell Biochem.* **84**(S37), 71–81 (2001).
18. P. Bao et al., "High-sensitivity detection of DNA hybridization on microarrays using resonance light scattering," *Anal. Chem.* **74**(8), 1792–1797 (2002).
19. R. F. Pasternack et al., "Porphyrin assemblies on DNA as studied by a resonance light-scattering technique," *J. Am. Chem. Soc.* **115**(13), 5393–5399 (1993).
20. W. S. Bickel et al., "Application of polarization effects in light scattering: a new biophysical tool," *Proc. Nat. Acad. Sci. U.S.A.* **73**(2), 486–490 (1976).
21. S. Schultz et al., "Single molecule detection with nonbleaching multi-color optical immunolabels," *Proc. Natl. Acad. Sci. U.S.A.* **97**(3), 996–1001 (2000).
22. T. A. Taton et al., "Scanometric DNA array detection with nanoparticle probes," *Science* **289**(5485), 1757–1760 (2000).
23. H. Wang et al., "In vitro and in vivo two-photon luminescence imaging of single gold nanorods," *Proc. Nat. Acad. Sci. U.S.A.* **102**(44), 15752–15756 (2005).
24. N. J. Durr et al., "Two-photon luminescence imaging of cancer cells using molecularly targeted gold nanorods," *Nano Lett.* **7**(4), 941–945 (2007).
25. C. Hubert et al., "Role of surface plasmon in second harmonic generation from gold nanorods," *Appl. Phys. Lett.* **90**(18), 181105 (2007).
26. L. Qiu et al., "Gold nanorod light scattering labels for biomedical imaging," *Biomed. Opt. Express* **1**(1), 135–142 (2010).
27. C. J. Orendorff et al., "Light scattering from gold nanorods: tracking material deformation," *Nanotechnology* **16**(11), 2601–2605 (2005).
28. A. M. Alkilany et al., "Cellular uptake and cytotoxicity of gold nanorods: molecular origin of cytotoxicity and surface effects," *Small* **5**(6), 701–708 (2009).
29. X. Huang et al., "Cancer cell imaging and photothermal therapy in the near-infrared region by using gold nanorods," *J. Am. Chem. Soc.* **128**(6), 2115–2120 (2006).
30. C. G. Wang et al., "Biorecognition-driven self-assembly of gold nanorods: a rapid and sensitive approach toward antibody sensing," *Chem. Mater.* **19**(24), 5809–5811 (2007).
31. D. I. Gittins et al., "Tailoring the polyelectrolyte coating of metal nanoparticles," *J. Phys. Chem. B* **105**(29), 6846–6852 (2001).
32. I. H. El-Sayed et al., "Surface plasmon resonance scattering and absorption of anti-EGFR antibody conjugated gold nanoparticles in cancer diagnostics: applications in oral cancer," *Nano Lett.* **5**(5), 829–834 (2005).
33. J. Yguerabide et al., "Light-scattering submicroscopic particles as highly fluorescent analogs and their use as tracer labels in clinical and biological applications. I. Theory," *Anal. Biochem.* **262**(2), 137–156 (1998).
34. J. Yguerabide, "Light-scattering submicroscopic particles as highly fluorescent analogs and their use as tracer labels in clinical and biological applications. II. Experimental characterization," *Anal. Biochem.* **262**(2), 157–176 (1998).
35. D. S. Wang et al., "Surface plasmon effects on two photon luminescence of gold nanorods," *Opt. Express* **17**(14), 11350–11359 (2009).
36. K. Imura et al., "Near-field two-photon-induced photoluminescence from single gold nanorods and imaging of plasmon modes," *J. Phys. Chem. B* **109**(27), 13214–13220 (2005).
37. G. T. Boyd et al., "Photoinduced luminescence from the noble metals and its enhancement on roughened surfaces," *Phys. Rev. B* **33**(12), 7923–7936 (1986).
38. V. K. Valev et al., "The role of chiral local field enhancements below the resolution limit of Second Harmonic Generation microscopy," *Opt. Express* **20**(1), 256–264 (2012).
39. Y. Garini et al., "From micro to nano: recent advances in high-resolution microscopy," *Curr. Opin. Biotech.* **16**(1), 3–12 (2005).
40. G. Malpuech et al., "Resonant Rayleigh scattering of exciton-polaritons in multiple quantum wells," *Phys. Rev. Lett.* **85**(3), 650–653 (2000).
41. P. Bianchini et al., "Single-wavelength two-photon excitation-stimulated emission depletion (SW2PE-STED) superresolution imaging," *Proc. Nat. Acad. Sci. U.S.A.* **109**(17), 6390–6393 (2012).
42. C. Zhang et al., "Reflection-mode submicron-resolution in vivo photoacoustic microscopy," *J. Biomed. Opt.* **17**(2), 020501 (2012).

43. D. Y. Joh et al., "On-chip Rayleigh imaging and spectroscopy of carbon nanotubes," *Nano Lett.* **11**(1), 1–7 (2011).
44. K. Sokolov et al., "Real-time vital optical imaging of precancer using anti-epidermal growth factor receptor antibodies conjugated to gold nanoparticles," *Cancer Res.* **63**(9), 1999–2004 (2003).
45. D. R. Larson et al., "Water-soluble quantum dots for multiphoton fluorescence imaging in vivo," *Science* **300**(5624), 1434–1436 (2003)
46. E. J. Yoder et al., "Cortical imaging through the intact mouse skull using two-photon excitation laser scanning microscopy," *Microsc. Res. Techniq.* **56**(4), 304–305 (2002).